Purcell factors and Förster-resonance energy transfer in proximity to helical structures

Asaf Farhi[1,2] and Aristide Dogariu[1]
[1]*CREOL, University of Central Florida, Orlando, Florida 32816, USA*
[2]*Department of Applied Physics, Yale University, New Haven, Connecticut 06520, USA*

(Received 19 October 2021; accepted 27 May 2022; published 13 July 2022)

Both spontaneous emission and resonant energy transfer can be enhanced significantly when the emitter is placed in the vicinity of metallic or crystal structures. This enhancement can be described using the electromagnetic Green tensor and is determined by the dominant surface modes of the structure. Here we use the eigenpermittivity formalism to derive the spontaneous emission and Förster-resonance energy transfer (FRET) rates in the quasistatic regime in a two-constituent medium with an anisotropic inclusion. We then apply our results to a helical structure supporting synchronous vibrations and evaluate the contribution of these modes, which are associated with a strong and delocalized response. We show that this contribution can result in large Purcell factors and long-range FRET, which oscillates with the helix pitch. These findings may have implications in understanding and controlling the interactions of molecules close to helical structures such as the microtubules.

DOI: 10.1103/PhysRevA.106.013708

I. INTRODUCTION

Helical structures like alpha helices, DNA, and microtubules have profound importance in biology. Microtubules (MTs) are composed of identical tubulin-dimer units and therefore they have a regular helical shape, similarly to carbon nanotubes [1]. MTs self-assemble from their constituent tubulin-protein units and are critical for the development and maintenance of the cell shape, transport of vesicles, and other components throughout cells, cell signaling, and mitosis. Tubulins have a large dipole moment [2–5] and it was suggested that MT vibrations could generate an electric field in its vicinity [6–8], also beyond the typical Coulomb and van der Waals range.

An optical system can generate a strong electromagnetic field for certain sets of physical parameters, which are the resonances of the system. An eigenvalue is a parameter of the system that corresponds to a resonance, and it can be obtained by fixing all the other parameters and imposing outgoing boundary conditions without a source. In electrodynamics the eigenvalue is usually defined as an eigenfrequency or eigenpermittivity of one of the constituents [9–11]. In the eigenfrequency formalism a resonance can be approached when the real physical frequency is close to the usually complex eigenfrequency. In the eigenpermittivity formalism a resonance can be achieved when the physical permittivity of one of the constituents is equal to a generally complex eigenpermittivity of that constituent.

For a simple system with two uniform and isotropic constituents as in Fig. 1(a), when the eigenpermittivity ratio ϵ_{1m}/ϵ_2 is equal to the physical permittivity ratio ϵ_1/ϵ_2, there is a strong response of the system. In the quasistatic (QS) regime, in which the typical length scale is much smaller than the wavelength, ϵ_{1m}/ϵ_2 are real and usually negative (see Appendix 1 and Refs. [12,13]). Hence, resonances can usually be approached when the permittivity of one of the constituents is positive and the permittivity of the other is negative, both with low loss. Examples include silver–polymethyl methacrylate [11,14], silver-water in the high-visible regime [15], graphene [16], and SiC [17]. In the full-Maxwell equation analysis, ϵ_{1m}/ϵ_2 is usually complex and approaching a resonance requires gain in one of the constituents [9,11].

In electrodynamics an eigenstate is an electric field that exists without a source and corresponds to an eigenvalue. Such eigenstates have been used to approximate the field at a resonance in the eigenfrequency formalism [10] and expand the scattered field in response to an applied field in a two-constituent medium in the eigenpermittivity formalism [9–11]. These field approximations and field expansions have been generalized to a dipole source excitation independently [10,11], which is of paramount importance for a variety of applications. Another approach for such a calculation is to expand the electric potential of a source in free space according to the inclusion geometry and impose boundary conditions for these modes and the scattered electric potential modes [18].

Recently, we have shown that in the QS regime when one of the constituents in a two-constituent medium is anisotropic as in Fig. 1(b) there is an infinite degeneracy of real eigenpermittivities, similarly to the situation in electrodynamics. In this case, however, the eigenpermittivities are real, which can lead to a strong response when an external field is applied. We then used the corresponding eigenfunctions to expand the field in such a setup [19].

When the structure is a crystal with a period a as in Fig. 1(c), one can use an effective $\epsilon(\boldsymbol{k})$ when $\lambda \gg a$ [20]. Assuming that $k \approx 0$ and $\epsilon(\omega)$, when the physical frequency is close to a resonant frequency $\omega \approx \omega_T$, the physical permittivity diverges to plus and minus infinity [17,21–23]. Thus, it can be equal to an eigenpermittivity and result in a strong response. This approximation can also be used in the QS regime when the source-structure distance l, which

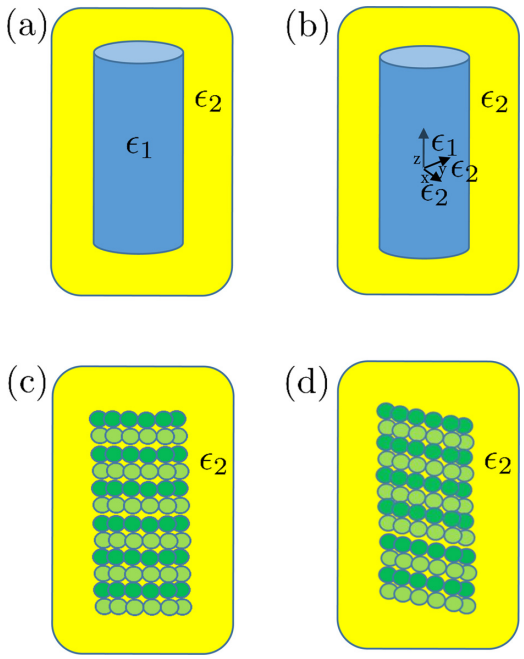

FIG. 1. (a) Dielectric cylindrical ϵ_1 structure in an ϵ_2 host medium. (b) Dielectric cylindrical structure with ϵ_1 in the z direction and ϵ_2 in the ϕ and ρ directions, in an ϵ_2 host medium. Note that even though the permittivity of the inclusion in the ϕ and ρ directions and the permittivity of the host are equal, the different axial permittivity of the inclusion defines an interface. This allows us to model axial vibrations as will be explained. Periodic longitudinal (c) and helical (d) arrangements of the constituent units. Panels (c) and (d) are realizations of (b) with $\epsilon_1(k)$ and their vibrational modes are longitudinal and helical, respectively [19,21].

is on the order of the effective wavelength [23], satisfies $l \gg a$.

The response of a helical structure of Fig. 1(d) to an incoming electric field due to the vibrational modes was recently studied in the QS regime. The arrangement of the units in a *helical periodicity* enabled us to write an effective permittivity $\epsilon_1(\boldsymbol{k})$. Then, in order to model axial vibrations we considered an effective permittivity in the axial axis $\epsilon_{1z}(\boldsymbol{k})$ and permittivity value in the other axes ϵ_2, the permittivity of the host medium. In this work we also investigated the permittivity when $k \geqslant 2\pi/a$, where a is the helix pitch. We identified synchronous-vibration modes satisfying $k = mk_z$, where m and k are the cylindrical-mode indices, and $k_z = 2\pi/a$. These modes were shown to have $\omega(k)$ that is close to real, which is associated with a strong response and delocalization. When the physical frequency $\omega \approx \omega(k)$, the permittivity is expected to span over a large range of values and give rise to resonances and delocalization [19], similarly to the scenario in crystals mentioned above. Interestingly, delocalized phonons were recently observed in DNA under physiological conditions [24].

The local density of states (LDOS) of the electromagnetic field is an important quantity since it determines the magnitude of light-matter interactions such as the spontaneous emission rate. The LDOS is proportional to the imaginary part of the Green tensor, which depends linearly on the electric field generated in response to a dipole excitation [25]. Hence, close to a resonance there is an increase of the scattered field and therefore in the LDOS, which in turn enhances light-matter interactions and spontaneous-emission rate [18,26,27]. To quantify this enhancement one can use the Purcell factor [28], which is defined as spontaneous emission rate in a given system relative to free space.

Moreover, when two dipoles are located in proximity to a structure, the Förster-resonance energy transfer (FRET) between them is also described in terms of the Green tensor [29]. Thus, close to a resonance, we should expect an enhancement in the FRET between the dipoles as well. In free space, such a FRET process between two dipoles is very short range, on the order of 3–4 nm. Thus, if a resonant helical structure can mediate FRET between dipoles spaced significantly further apart, it would be of utmost importance in understanding and controlling molecular interactions in the vicinity of such a structure.

Here we will first evaluate the LDOS and the FRET rate between two dipoles in the vicinity of an *anisotropic* structure using the eigenpermittivity formalism. We will then apply the results to the case of a generic helical structure supporting axial vibrations and discuss the consequences for strong light-matter interaction, high frequency selectivity, and structure-mediated long-range energy transfer between dipoles. Importantly, we will calculate the interaction between a crystal and a dipole source and between a crystal and electric field with an effective wavelength on the order of the length period of the crystal, which in our case is due to the proximity of the dipole to the structure [30]. For concreteness, we will consider the microtubule, which also has axial periodicity [19].

II. CALCULATING THE LDOS AND FRET RATES IN PROXIMITY TO AN ANISOTROPIC STRUCTURE

We start by expanding the electric field using the eigenpermittivity formalism in the QS regime for a two-constituent system comprising an *isotropic* cylindrical inclusion in a host medium and a point-dipole source situated in the host medium. An electric potential expansion and Purcell enhancement for such a setup using mode matching were calculated in Ref. [18]. The field generated by the dipole at a position $\boldsymbol{r}$ is

$$E_\mu = \sum_m \frac{L_z}{2\pi} \int dk' \frac{s_{mk'}^2}{s - s_{mk'}} \frac{\nabla \psi_{mk'}^*(\boldsymbol{r}_0) \cdot \boldsymbol{p}}{\langle \psi_{mk'} | \psi_{mk'} \rangle} [\nabla \psi_{mk'}(\boldsymbol{r})]_\mu, \quad (1)$$

where $s = \frac{\epsilon_2}{\epsilon_2 - \epsilon_1}$, $s_m = \frac{\epsilon_2}{\epsilon_2 - \epsilon_{1m}}$, $\boldsymbol{p}$ is the dipole moment, $\boldsymbol{r}_0$ is the dipole location, $\psi_{mk'}$ are the quasielectric potential eigenfunctions, μ is the field direction, $\langle \psi_{mk'} | \psi_{mk'} \rangle = \int \theta_1 \nabla \psi_{mk'} \cdot \nabla \psi_{mk'} d\boldsymbol{r}$, θ_1 is a window function that equals 1 inside the inclusion volume, and L_z is an arbitrary length that cancels out with L_z in $\langle \psi_{mk'} | \psi_{mk'} \rangle$ [11,12,15,19]. Note that when $\epsilon_1 \approx \epsilon_{1m}$ there is a large contribution of the corresponding mode in the field expansion.

This formulation was recently generalized to the case of an anisotropic inclusion by assigning ϵ_1 to one axis and ϵ_2 to the other two axes to model axial vibrations and we can proceed accordingly with $\epsilon_1 \to \epsilon_{1z}$ and the corresponding eigenfunctions [see Fig. 1(b) and Ref. [19]]. The Green tensor

is proportional to the electric field generated by a dipole and can be expressed as [25]

$$G_{\mu\mu'} = \frac{E_\mu e_{p\mu'}}{\omega^2 p} = \frac{E_\mu e_{p\mu'}}{k^2 c^2 p}, \quad k = \frac{2\pi}{\lambda},$$

and therefore we readily obtain the expression for the Green function:

$$G_{\mu\mu'}(\boldsymbol{r}, \boldsymbol{r}_0) = \frac{1}{\omega^2} \sum_m \frac{L_z}{2\pi} \int dk' \frac{s_{mk'}^2}{s - s_{mk'}} \frac{\nabla \psi_{mk'}^*(\boldsymbol{r}_0) \cdot \boldsymbol{e}_{\mu'}}{\langle \psi_{mk'} | \psi_{mk'} \rangle} [\nabla \psi_{mk'}(\boldsymbol{r})]_\mu. \tag{2}$$

This expression can then be used to derive the cross density of states (CDOS) [25]:

$$\overline{\rho}(\boldsymbol{r}, \boldsymbol{r}_0) = -\frac{2\omega}{\pi} \mathrm{Im}[G_{\mu\mu}(\boldsymbol{r}, \boldsymbol{r}_0)]. \tag{3}$$

Similarly, the FRET rate between dipoles at $\boldsymbol{r}_A$ and $\boldsymbol{r}_B$ can be written as [29]

$$w_{ab'}^{a'b} = \frac{2\pi}{\hbar^2} \left(\frac{\omega_{a'a}}{\epsilon_0 c^2} \right)^2 |\mathbf{p}_{b'b} \overleftrightarrow{G}(\boldsymbol{r}_B, \boldsymbol{r}_A, \omega_{a'a}) \mathbf{p}_{aa'}|^2, \tag{4}$$

and we arrive at

$$w_{ab'}^{a'b} = \frac{2\pi}{\hbar^2} \left(\frac{1}{\epsilon_0 c^2} \right)^2 \left(\frac{1}{\omega} \frac{L_z}{2\pi} \right)^2 \left| \sum_m \times \int dk' \frac{s_{mk'}^2}{s - s_{mk'}} \frac{\nabla \psi_{mk'}^*(\boldsymbol{r}_B) \cdot \boldsymbol{p}_{aa'} \nabla \psi_{mk'}(\boldsymbol{r}_A) \cdot \boldsymbol{p}_{bb'}}{\langle \psi_{mk'} | \psi_{mk'} \rangle} \right|^2. \tag{5}$$

Assuming a sharp resonance and using the identity $\delta(x) = \lim_{\epsilon \to 0} \frac{1}{\pi} \frac{\epsilon}{x^2 + \epsilon^2}$, similarly to the spontaneous-emission rate calculation in Ref. [27], one can readily solve analytically the integrals in Eqs. (3) and (5).

The LDOS, which is a particular case of the CDOS for $\boldsymbol{r} = \boldsymbol{r}_0$, defined as [22,23,30,31]

$$\overline{\rho}_\mu(\boldsymbol{r}) = -\frac{2\omega}{\pi} \mathrm{Im}[G_{\mu\mu}(\boldsymbol{r}, \boldsymbol{r})], \tag{6}$$

can also be obtained:

$$\overline{\rho}_\mu = -\frac{2}{\pi} \frac{1}{\omega} \times \sum_m \int dk' \frac{s_m^2 \mathrm{Im}(s^*)}{[\mathrm{Re}(s) - s_m]^2 + [\mathrm{Im}(s)]^2} \frac{|\nabla \psi_{m\mu}|^2}{\langle \psi_m | \psi_m \rangle}. \tag{7}$$

By expressing the spontaneous emission rate in a general setup [22]

$$\Gamma = \frac{\pi \omega_{eg} p^2}{\hbar \epsilon_0} \overline{\rho}_\mu(\boldsymbol{r}, \omega) \propto \omega_{eg} \overline{\rho}_\mu, \tag{8}$$

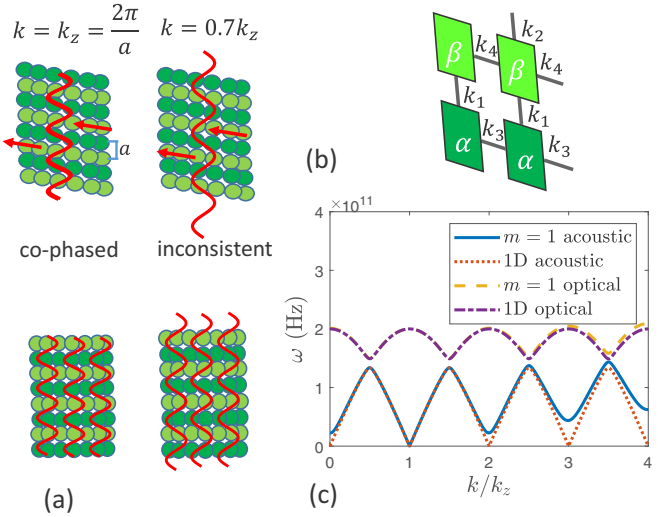

FIG. 2. Vibrational-mode analysis for a helical structure. (a) The illustrations show that $k = k_z m$ are allowed when requiring decoupling between the axial protofilaments. (b) The structure is composed of two units denoted by α, β with masses m_1, m_2 connected with springs k_1, k_2, k_3, k_4. (c) $\omega(k)$ for the acoustic and optical $m = 1$ helix and 1D crystal modes. The microtubule parameters are $m_1 = m_2 = 0.9 \times 10^{-22}$ (Kg), $k_1 = 0.8$, $k_2 = 0.1$, $k_3 = k_4 = 0.2$ (N/m), where k_4 is of the order of magnitude of the value in Ref. [36].

where ω_{eg} is the Bohr frequency between the ground and excited states, and the corresponding one in vacuum [22]

$$\Gamma_{\mathrm{vacuum}} = \frac{\omega_{eg}^3}{3\pi \hbar \epsilon_0 c^3} p^2, \tag{9}$$

we get the following expression for the Purcell factor:

$$\frac{\Gamma}{\Gamma_{\mathrm{vacuum}}} = \frac{3\pi^2 c^3 \overline{\rho}_{e,u}(\boldsymbol{r}, \omega)}{\omega_{eg}^2} = -3\pi \frac{1}{k^3} 2 \sum_m \int dk' \times \frac{s_m^2 \mathrm{Im}(s^*)}{\{\mathrm{Re}[s(k')] - s_m(k')\}^2 + [\mathrm{Im}(s)]^2} \frac{|\nabla \psi_{m,k'\mu}(\boldsymbol{r}_0)|^2}{\langle \psi_m | \psi_m \rangle}. \tag{10}$$

III. APPLYING THE CALCULATION TO HELICAL STRUCTURES

We will now examine the specific case of a helical structure supporting synchronous-vibration modes, which can give rise to resonances. The scattering QS eigenfunctions that correspond to these vibrations satisfy the relation $k = mk_z$ due to their functional dependency, that is, according to the helical symmetry, as illustrated in Fig. 2(a), and can be expressed as [19]

$$\psi_m = e^{im(k_z z - \phi)} \begin{cases} A_{4m} K_m(mk_z \rho) & \rho > \rho_2 \\ A_{2m} K_m\left(mk_z \sqrt{\frac{\epsilon_{1zm}}{\epsilon_2}} \rho\right) + A_{3m} I_m\left(mk_z \sqrt{\frac{\epsilon_{1zm}}{\epsilon_2}} \rho\right) & \rho_1 < \rho < \rho_2 \\ A_{1m} I_m(mk_z \rho) & \rho < \rho_1 \end{cases}, \tag{11}$$

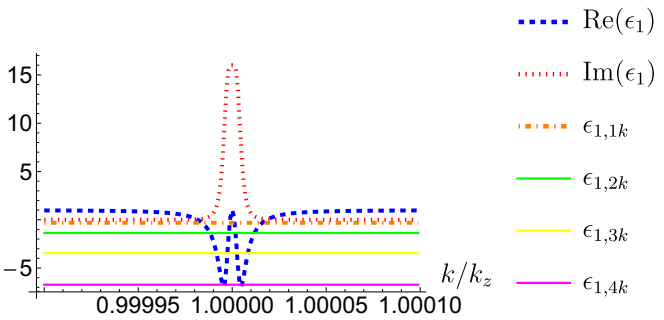

FIG. 3. Physical permittivity $\epsilon_1(k)$ and first eigenpermittivities $\epsilon_{1,nk}$ of the helical structure, where we used the parameters of Fig. 2 and $\rho_1 = 7$, $\rho_2 = 12$ nm. The real parts of the physical permittivity and the first eigenpermittivity intersect at two k values with $\mathrm{Im}(\epsilon_1) = 0.1i$, resulting in large contributions of the corresponding eigenfunctions. Note that we consider a single ω, and k in the QS expansion can take any value and is not required to satisfy $kv = \omega$.

where ρ_1 and ρ_2 are the internal and external inclusion radii, respectively, and I_m and K_m are the modified Bessel functions. The convergence of Eq. (10) is ensured since $K_{m\geqslant 1}(mk\rho \gg a) \to \frac{1}{\sqrt{2mk}}\sqrt{\frac{\pi}{\rho}}e^{-mk\rho}$, $\rho_0 > \rho_2$, and there is always an imaginary part of the permittivity (see Appendix 3).

In crystals, the permittivity is usually expanded in a Fourier series and it couples each field mode with the modes with $\mathbf{k} + \mathbf{G}_n$, where $\mathbf{G}_n$ is a reciprocal-lattice vector, and there is an effective $\overleftrightarrow{\epsilon_1}(\omega, \mathbf{k})$ that describes the $\omega, \mathbf{k}$ response to an excitation at $\omega, \mathbf{k}$ [20,32]. In our case, the symmetry to discrete translations defines the $k = mk_z$ and nk_z modes, where n is the number of units per helical round, that represent the dc and higher-order Fourier components, respectively (see also the static case of electric charges in a helical arrangement in Ref. [33]). Thus, the coupling is to modes with integer multiples of $(\Delta m, \Delta k) = (1, k_z)$ and $\Delta k = nk_z$ apart. At dipole distances on the order of the length period a, the field that is generated by the high-order modes is negligible at the dipole location and therefore the most dominant mode is the $m = 1$ mode.

We now analyze classically the vibrational modes that can be excited by the incoming field and generate field as was done in Ref. [19]. We consider the coupling of vibrations also to field components with $kc \gg \omega$ that are almost static [20] and satisfy $ka \geqslant 1$. When vibrational modes and electric field are coupled they have the same ω and $\mathbf{k}$, and, at low and high ks, $\omega(k)$ of one of the polaritons and that of the uncoupled vibrational mode are similar [21]. We study a structure comprising two types of units with masses m_1 and m_2 connected by springs $k_1, k_2, k_3,$ and k_4 as shown in Fig. 2(b). Denoting the axial displacements of $m_{1,2}$ and the indices of the axial and lateral shifts by $u_{1,2}$ and s, q, respectively, and assuming $u_{1,2} = a_{1,2}e^{ikz+im\phi}$, we write the equations of motion (EOM):

$$\begin{aligned} -\omega^2 m_1 u_{1sq} &= k_1(u_{2sq} - u_{1sq}) - k_2(u_{1sq} - u_{2s-1q}) - k_3(u_{1sq} - u_{1sq+1}) - k_3(u_{1sq} - u_{1sq-1}), \\ -\omega^2 m_2 u_{2sq} &= k_2(u_{1s+1q} - u_{2sq}) - k_1(u_{2sq} - u_{1sq}) - k_4(u_{2sq} - u_{2sq+1}) - k_4(u_{2sq} - u_{2sq-1}), \end{aligned} \tag{12}$$

$$\begin{pmatrix} -\omega^2 m_1 + k_1 + k_2 + 4k_3 \sin^2((ka/n - 2\pi m/n)/2) & -(k_2 e^{-ika} + k_1) \\ -(k_2 e^{ika} + k_1) & -\omega^2 m_1 + k_1 + k_2 + 4k_4 \sin^2((ka/n - 2\pi m/n)/2) \end{pmatrix} \begin{pmatrix} u_1 \\ u_2 \end{pmatrix} = \begin{pmatrix} 0 \\ 0 \end{pmatrix}. \tag{13}$$

This one-dimensional (1D) description enables us to analyze the behavior of the system in the axial axis while accounting for the lateral interactions in the terms with k_3 and k_4. These diagonal terms restrain the movements of m_1 and m_2 to their sites as in a local oscillator and vanish for the helical functions satisfying $k = mk_z$ [see Eq. (11)]. Also, for these modes it can be seen that laterally adjacent units oscillate in phase. Equation (13) can be written as $A\mathbf{u} = \omega^2\mathbf{u}$, where A is a Hermitian matrix and therefore diagonalizable and since ω^2 is real and positive the modes are delocalized. When anharmonicity or dissipation is incorporated, the matrix formulation and Hermiticity no longer hold and localization can arise. We assume that the largest anharmonicity is in the axial forces between lateral units due to the alignment shift of the units upon movement and the distribution of charge along them (see Ref. [19] Fig. A1). The anharmonicity in these terms $\propto k_5 u_{1sq}^2\{1 - 2\cos(ka/n - 2\pi m/n) + \cos[2(ka/n - 2\pi m/n)]\}$ and translates to an *on-site* anharmonic term, which vanishes for the $k = mk_z$ modes. Moving away from $k = mk_z$ increases the ratio of anharmonicity to dispersion, leading to a more localized response, similarly to interacting diatomic molecules with *internal* anharmonicity [34,35]. From Eq. (13) we calculate $\omega(k)$ for the acoustic and optical modes without anharmonicity. The $k = mk_z$ modes have the same $\omega(k)$ of a 1D crystal [see Fig. 2(c)] in agreement with the previous analysis in Eq. (11). We then incorporated dissipation into the calculation of $\omega(k)$, which showed that $\mathrm{Re}[\omega(k)]$ is hardly affected and $\mathrm{Im}[\omega(k)]$ is constant at all ks, except at large γs that suppress the acoustic modes (see Ref. [19] Appendix B3). The physical permittivity can then be written similarly to the derivation for a harmonic oscillator [21] with the oscillator eigenfrequency $\omega_T \to \omega(\mathbf{k})$ [19]:

$$\epsilon_1 = 1 + \frac{4\pi N q^2}{m_r[\omega^2(\boldsymbol{k}) - \omega^2]}, \tag{14}$$

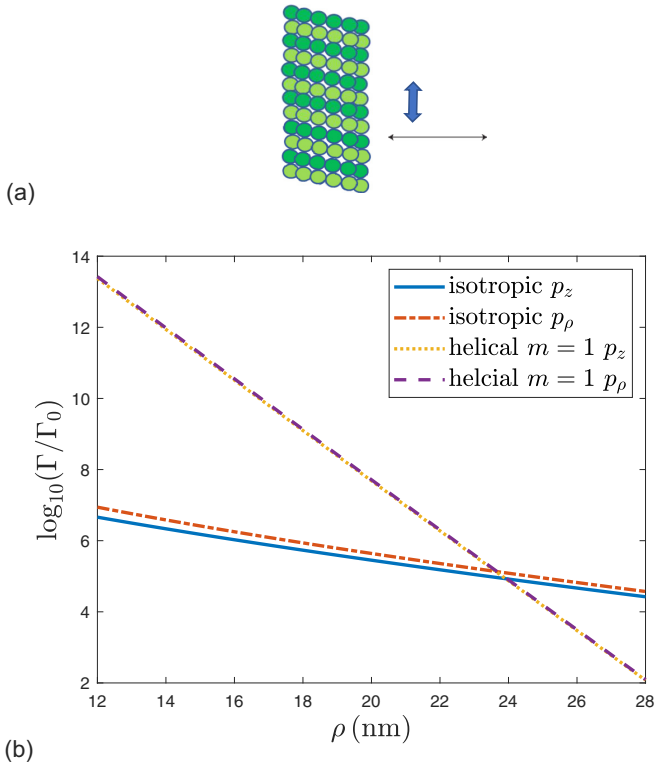

FIG. 4. (a) A setup of a dipole in proximity to a helical structure where the spontaneous emission rate of the dipole is enhanced due to the proximity to the structure. (b) Purcell factors in the z and ρ directions as functions of the radius for isotropic and helical structures with $\rho_1 = 7$ nm and $\rho_2 = 12$ nm, where the helical structure has $a = 8$ nm. The Purcell factors in the ϕ direction are smaller by at least an order of magnitude since $1/\rho < k$, except at close distances to the isotropic structure, where the magnitudes are negligible compared with the helical structure. The Purcell factors of the helical structure are dominant for $12 < \rho < 24$ nm and the ones of the isotropic structure are dominant for $\rho > 24$ nm. In addition, the Purcell factors in the ρ direction are larger for the isotropic structure whereas the magnitudes in the ρ and z directions are similar for the helical structure.

where q is the unit charge, m_r is the effective mass, and N is the charge density. Note that in electrodynamics in the quasistatic regime, the dependency on ω is negligible and therefore the polariton eigenfrequency is approximately determined by the vibrational modes.

We are now in a position to derive the LDOS and the FRET rate for helical structures using the expressions in Eqs. (5) and (7). For simplicity we focus on the $m = 1$ modes, which dominate at large distances, and proceed without anharmonic terms [19], similarly to Ref. [21]. We first calculate $\epsilon_1(k)$ and ϵ_{1k} using the expression above and the boundary conditions [19], respectively, to observe the intersection points between them, which are the resonances. In the calculation of $\epsilon_1(k)$ we chose $q = 12e$, where e is the electron charge [37], and spring constants on the order of the one reported in Ref. [38]. We also use in the expression of $\epsilon_1(k)$, $\omega^2(\boldsymbol{k})$ that incorporates dissipation and has a constant imaginary part [19]. To compare the LDOS and FRET results to an isotropic dielectric structure (which is the standard modeling of helical structures of this kind), with $\epsilon_1 = 1.5 + 0.1i$, we set $\mathrm{Im}(\omega_n) = \frac{\pi N q^2}{4m_r}$, which satisfies $\mathrm{Im}(\epsilon_1) = 0.1i$ at an intersection point. Then, using $\epsilon_1(k)$ and ϵ_{1k}, we perform the calculation of the LDOS and FRET for the helical structure setup and compare the results. For details about the calculations for the isotropic structure see Appendix 5.

In Fig. 3 we present the physical permittivity ϵ_1 and the eigenpermittivities ϵ_{1k} for the first few modes of the helical structure. Due to the anisotropy there is an infinite number of eigenpermittivities for a given k value, unlike the case of an isotropic medium. While this resembles electrodynamics, in which there are are multiple resonances at a given k value, the eigenpermittivities in this case are real and can give rise to a strong response, especially for the first resonances where $\mathrm{Im}(\epsilon_1)$ is small. Since the resonances are discrete, if we assume that each resonance is a continuous function of ω and k, when varying ω we will encounter closely spaced resonances (one can think of resonances represented by, e.g., parallel diagonal lines in ω and k). This is in qualitative agreement with the closely spaced resonances in frequency in the experimental results in Ref. [39].

In Fig. 4 we present the Purcell factors in the z and ρ directions, which are the dominant ones, as functions of ρ for the helical and isotropic structures, both with $\rho_1 = 7$ nm, $\rho_2 = 12$ nm. It can be seen that for the isotropic structure the magnitudes in the ρ direction are larger, whereas for the helical structure the magnitudes in the ρ and z directions are similar. Interestingly, close to the structure the LDOS of the helical structure dominates since the $m = 1$ modes that extend the farthest have a larger response compared to the isotropic structure, while at some distance away the response of the isotropic

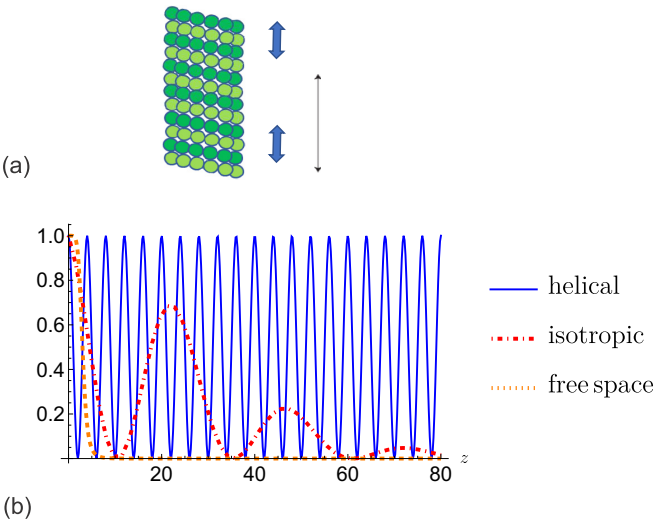

FIG. 5. (a) The setup of two dipoles in proximity to the helical structure, which can transfer energy via the structure. (b) Normalized FRET rates as functions of the axial distance between two dipoles oriented in the z direction for an isotropic dielectric structure with $\epsilon_1 = 1.5 + 0.1i$, helical structure, and free space. The distance of the dipoles from the structures is a, which is the helix pitch.

structure is larger. This can be explained by the strong response of the helical structure up to an interaction distance on the order of a due to the synchronous-vibration modes, which depend on ρ via $K(k_z\rho)$ [see Eq. (11)]. In addition, the modes with larger interaction distances, which have small ks, are present in the isotropic structure but not in the helical structure since $\epsilon_1 \approx 1 \Rightarrow 1/(s - s_k) \approx 0$, and therefore they have a negligible contribution in the field expansion [see Eq. (2)]. This may suggest two distinct mechanisms of interaction in these regions. Finally, we note that Purcell factors depend on the frequency as follows: $\Gamma/\Gamma_0 \propto 1/\omega^3$ [see Eq. (10)]. Since in our case $\omega = 2 \times 10^{11}$ (s^{-1}), it gives, e.g., an additional factor of 5×10^8 compared to the calculation in the near infrared in Fig. 3 of Ref. [27].

In Fig. 5 we present the normalized FRET rates between two axially distanced dipoles oriented in the z direction at a distance a from the helical and isotropic structures as well as in free space. The isotropic structure exhibits a larger FRET range compared to free space, similarly to a Gaussian beam in which the modes interfere. Importantly, at a given time the FRET close to the helical structure setup has an approximately constant amplitude and oscillates with a period a, due to the $\exp(ik_z z)$ dependency in Eq. (11). Note that since we have incorporated dissipation into the permittivity the FRET rate in this model decays in space, at a distance that is larger than the one displayed in the graph and can be approximated using $\Delta x \approx 1/(\sqrt{2}\Delta k)$, where Δk is according to the integrand in Eq. (5). We also calculated the FRET rates for dipoles oriented along the ρ and ϕ directions and in the helical-structure setup, they have approximately the same z dependency since the contribution is dominated by $\exp(ik_z z)$ [see Eq. (11)], and their relative magnitudes are 1.14 and 1.64×10^{-5}, respectively. The scaling of the FRET as a function of the dipole radius for dipoles oriented along z, ρ, and ϕ at distances on the order of a or larger can be approximated as $[k_z K_1(k_z\rho)]^2$, $[K_1'(k_z\rho)]^4$, and $[\frac{1}{\rho}K_1(k_z\rho)]^4$, respectively. Finally, the FRET rate as a function of z between dipoles oriented along z and ρ in the helical-structure setup is shifted in phase by $\pi/2$, which implies that for dipoles at the same z location the FRET rate will be maximal when they are parallel. Incorporating the induced electric response and the anharmonic terms is expected to result in a shorter FRET distance close to the helical structure. Clearly, the effect of including the anharmonic terms depends on their coefficients and the strength of the incoming field, which will determine the mode amplitude. Usually, on a resonance since the mode amplitude is large and the anharmonic terms are significant, it will increase the imaginary part of ω_k, which in turn will reduce the strength and axial extent of the response since ω is real. However, assuming that the dominant anharmonicity is in the axial forces between lateral units, this effect is expected to be dominant only away from the modes satisfying $k = mk_z$, where this anharmonicity is large. Thus, excitation at an ω that is significantly different than $\omega_k(k = mk_z)$ will result in a weaker and more localized response, see Appendix 6. Additional anharmonic terms can decrease the FRET range.

IV. CONCLUSION

In this work we first derived the density of states, Purcell factors, and FRET rate in the eigenpermittivity formalism for a two-constituent system with isotropic and anisotropic inclusions. We then applied this formulation to the case of a helical structure supporting axial vibrations and compared it with an isotropic dielectric structure. We showed that the helical structure can greatly enhance the spontaneous emission rate up to distances on the order of the helix pitch and that at much larger distances the dielectric response dominates. Finally, we showed that helical structures can mediate long-range FRET between two dipoles. This could be crucial for understanding and controlling molecular interactions in the vicinity of such structures. Our results may be of particular relevance for phenomena associated with biological helical structures such as DNA, microtubules, and alpha helices, and could relate to fundamental questions in biology such as the role of electrodynamics in explaining long-range interactions and synchronization between distant molecules.

APPENDIX

1. Expansion of the potential of a dipole for an anisotropic and spatially-dispersive inclusion

We will start by expanding the physical potential of a charge distribution in a two-constituent medium, in which both constituents are isotropic and spatially uniform, similarly to the treatment in Refs. [11,12,40]. We will then develop an expansion for an inclusion with an anisotropic and spatially uniform permittivity and simplify it for a dipole source. Finally, we will formulate the field expansion for a k-dependent inclusion permittivity where the modes are uncoupled and analyze the scattered field for a crystal inclusion.

In the quasistatic regime we use Poisson's equation in a two-constituent medium for the electric potential of a charge distribution $\tilde{\rho}(\mathbf{r})$. When both constituents have spatially uniform and isotropic permittivities we write [11,12,40]

$$\nabla\epsilon\nabla\psi = \tilde{\rho}(\mathbf{r}),$$

$$\nabla^2\psi(\mathbf{r}) = \nabla\cdot\theta_1(\mathbf{r})u\nabla\psi(\mathbf{r}) + \tilde{\rho}(\mathbf{r})/\epsilon_2, \quad u \equiv \frac{\epsilon_2-\epsilon_1}{\epsilon_2},$$

where $\theta_1(\mathbf{r})$ is a window function that equals 1 inside the inclusion, ϵ_1 is the inclusion permittivity, and ϵ_2 is the host-medium permittivity. The potential can be regarded as generated by the external charge distribution $\tilde{\rho}(\mathbf{r})/\epsilon_2$ and $\nabla\cdot\theta_1(\mathbf{r})u\nabla\psi(\mathbf{r})$. Therefore, it can also be expressed as $\psi = \psi_0 + \psi_{\rm sc}$ in terms of the potential ψ_0 generated by the charge distribution in a uniform ϵ_2 medium and $\psi_{\rm sc}$ that is generated due to the existence of the inclusion.

An eigenstate ψ_n, which exists in a system without a source, is defined as follows:

$$\nabla^2\psi_n(\mathbf{r}) = \nabla\cdot\theta_1(\mathbf{r})u_n\nabla\psi_n(\mathbf{r}), \quad u_n \equiv \frac{\epsilon_2-\epsilon_{1n}}{\epsilon_2},$$

$$\psi_n(\mathbf{r}) = \int G(\mathbf{r}-\mathbf{r}')\nabla\cdot\theta_1 u_n\nabla\psi_n(\mathbf{r}')d\mathbf{r}'$$

$$= u_n\int\theta_1(\mathbf{r}')\nabla G(\mathbf{r}-\mathbf{r}')\nabla\psi_n(\mathbf{r}')d\mathbf{r}',$$

where $G(\mathbf{r}-\mathbf{r}')$ is Green's function of Poisson's equation and we performed integration by parts. We define the operator $\hat{\Gamma}$ as

$$\hat{\Gamma}\psi_n = \int\theta_1(\mathbf{r}')\nabla G(\mathbf{r}-\mathbf{r}')\nabla\psi_n(\mathbf{r}')d\mathbf{r}'$$

and write

$$\psi_n = u_n\hat{\Gamma}\psi_n, \quad s_n\psi_n = \hat{\Gamma}\psi_n, \quad s_n = \frac{1}{u_n}.$$

Since $\hat{\Gamma}$ is self-adjoint all the eigenvalues s_n are real. In addition, at the large n limit $s_n = 1/2$ and therefore $\epsilon_1/\epsilon_2 = -1$ is an accumulation point of the eigenpermittivity ratios [12,13,40]. We then obtain [11,12,40]

$$\psi = u\hat{\Gamma}\psi + \psi_0$$

$$= \frac{1}{1-u\hat{\Gamma}}\psi_0 = \psi_0 + \frac{u\hat{\Gamma}}{1-u\hat{\Gamma}}\psi_0$$

$$= \psi_0 + \sum_n\frac{u\hat{\Gamma}}{1-u\hat{\Gamma}}|\psi_n\rangle\langle\psi_n|\psi_0\rangle$$

$$= \psi_0 + \sum_n\frac{s_n}{s-s_n}|\psi_n\rangle\langle\psi_n|\psi_0\rangle.$$

By using [11,15]

$$\langle\psi_n|\psi_0\rangle = \int d\mathbf{r}\theta_1\nabla\psi_n^*\cdot\nabla\psi_0$$

$$= \int d\mathbf{r}\theta_1(\mathbf{r})\nabla\psi_n^*(\mathbf{r})\cdot\nabla\int G(\mathbf{r}-\mathbf{r}')q\delta(\mathbf{r}'-\mathbf{r}_0)d\mathbf{r}'$$

$$= qs_n\int d\mathbf{r}'\psi_n^*(\mathbf{r}')q\delta(\mathbf{r}'-\mathbf{r}_0) = qs_n\psi_n^*(\mathbf{r}_0),$$

we get for a point charge

$$\psi = \psi_0 + q\sum_n\frac{s_n^2}{s-s_n}|\psi_n\rangle\psi_n^*(\mathbf{r}_0).$$

The eigenstates are assumed to be normalized, where the inner product is defined as

$$\langle\psi_n|\psi_n\rangle = \int d\mathbf{r}\theta_1\nabla\psi_n^*\cdot\nabla\psi_n.$$

Now we develop the expansion of the potential for an anisotropic inclusion permittivity as was done in Ref. [19]. We denote the inclusion permittivity tensor by $\overleftrightarrow{\epsilon_1}$ and write

$$\nabla\overleftrightarrow{\epsilon}\nabla\psi = \tilde{\rho}(\mathbf{r}),$$

$$\epsilon_2\nabla^2\psi + \nabla\theta_1(\overleftrightarrow{\epsilon_1}-\epsilon_2)\nabla\psi = \tilde{\rho}(\mathbf{r}),$$

$$\epsilon_2\nabla^2\psi = \frac{\tilde{\rho}(\mathbf{r})}{\epsilon_2} + \nabla\theta_1\frac{(\epsilon_2-\overleftrightarrow{\epsilon_1})}{\epsilon_2}\nabla\psi,$$

$$\nabla^2\psi(\mathbf{r}) = \nabla\cdot\theta_1(\mathbf{r})\overleftrightarrow{u}\nabla\psi(\mathbf{r}) + \frac{\tilde{\rho}(\mathbf{r})}{\epsilon_2},$$

$$\overleftrightarrow{u} \equiv \frac{\epsilon_2 I - \overleftrightarrow{\epsilon_1}}{\epsilon_2}$$

where I is the unit matrix.

We define an eigenfunction ψ_k as follows:

$$\psi_k(\mathbf{r}) = \int G(\mathbf{r}-\mathbf{r}')\nabla\cdot\theta_1\overleftrightarrow{u}\nabla\psi_k(\mathbf{r}')d\mathbf{r}'$$

$$= \int G(\mathbf{r}-\mathbf{r}')\frac{\partial}{\partial' i}\theta_1 u_{k,ij}\frac{\partial}{\partial' j}\psi_k(\mathbf{r}')d\mathbf{r}'$$

$$= \sum_{i,j}u_{ij,k}G(\mathbf{r}-\mathbf{r}')\frac{\partial}{\partial'_i}\theta_1(\boldsymbol{r}')\frac{\partial}{\partial'_j}\psi_k(\mathbf{r}')d\mathbf{r}'$$

$$= \sum_{i,j}u_{ij,k}\theta_1(\boldsymbol{r}')\frac{\partial}{\partial'_i}G(\mathbf{r}-\mathbf{r}')\frac{\partial}{\partial'_j}\psi_k(\mathbf{r}')d\mathbf{r}',$$

where we performed integration by parts and $u_{ij} \equiv \delta_{ij} - \frac{\epsilon_{1ij}}{\epsilon_2}$.

For a diagonal form of $\overleftrightarrow{\epsilon}$ we have

$$\psi_k(\mathbf{r}) = u_{i,k}\int G(\mathbf{r}-\mathbf{r}')\frac{\partial}{\partial'_i}\theta_1(\mathbf{r}')\frac{\partial}{\partial'_i}\psi_k(\mathbf{r}')d\mathbf{r}'$$

$$= \sum_i u_{i,k}\int\theta_1(\mathbf{r}')\frac{\partial}{\partial'_i}G(\mathbf{r}-\mathbf{r}')\frac{\partial}{\partial'_i}\psi_k(\mathbf{r}')d\mathbf{r}'.$$

For $(\epsilon_x,\epsilon_y,\epsilon_z) = (\epsilon_2,\epsilon_2,\epsilon_{1z})$ we get

$$\psi_k(\mathbf{r}) = u_{zk}\int G(\mathbf{r}-\mathbf{r}')\frac{\partial}{\partial'_z}\theta_1(\mathbf{r}')\frac{\partial}{\partial'_z}\psi_k(\mathbf{r}')d\mathbf{r}'$$

$$= u_{zk}\int\theta_1(\mathbf{r}')\frac{\partial}{\partial'_z}G(\mathbf{r}-\mathbf{r}')\frac{\partial}{\partial'_z}\psi_k(\mathbf{r}')d\mathbf{r}',$$

and write the eigenvalue equation

$$\psi_k = u_{zk}\hat{\Gamma}_z\psi_k, \quad s_{zk}\psi_k = \hat{\Gamma}_z\psi_k,$$

$$s_{zk} = 1/u_{zk} = \epsilon_2/(\epsilon_2-\epsilon_{1zk}),$$

where s_{zk} is an eigenvalue. Note that here the physical permittivity of the inclusion ϵ_1 is spatially uniform and the index k

denotes the mode index. Similarly, we write the expansion of ψ for this case

$$\psi = \psi_0 + \sum_k \frac{s_{zk}}{s_z - s_{zk}} |\psi_n\rangle\langle\psi_n|\psi_0\rangle.$$

For a point charge we substitute the eigenvalue equation in the inner product to obtain

$$\begin{aligned}\langle\psi_k|\psi_0\rangle &= \int d\mathbf{r}\theta_1(\mathbf{r})\frac{\partial}{\partial z}\psi_k^*(\mathbf{r})\frac{\partial}{\partial z}\psi_0(\mathbf{r}) \\ &= \frac{4\pi}{\epsilon_2}\int d\mathbf{r}\theta_1(\mathbf{r})\frac{\partial}{\partial z}\psi_k^*(\mathbf{r})\frac{\partial}{\partial z}G(\mathbf{r}-\mathbf{r}') * q\delta(\mathbf{r}'-\mathbf{r}_0) \\ &= \frac{4\pi q}{\epsilon_2}s_{zk}\psi_k^*(\mathbf{r}_0).\end{aligned}$$

We then consider a dipole composed of two charges and write

$$\begin{aligned}\langle\psi_k|\psi_0\rangle &= s_{zk}q[\psi_k^*(\mathbf{z}_0+\mathbf{d}/2) - \psi_k^*(\mathbf{z}_0-\mathbf{d}/2)] \\ &= s_{zk}qd\frac{[\psi_k^*(\mathbf{z}_0+\mathbf{d}/2) - \psi_k^*(\mathbf{z}_0-\mathbf{d}/2)]}{d}.\end{aligned}$$

For a cylindrical inclusion, the eigenfunctions have two indices, m and k. All in all, we obtain for ψ

$$\psi = \psi_0 + \frac{4\pi}{\epsilon_2}\sum_m \int \frac{s_{zk}^2}{s_z - s_{zk}} |\psi_{m,k}\rangle\nabla\psi_{m,k}^*(\mathbf{r}_0)\cdot\mathbf{p}dk, \tag{A1}$$

where the inner product for the normalization is

$$\langle\psi_k|\psi_k\rangle = \int d\mathbf{r}\theta_1(\mathbf{r})\frac{\partial}{\partial z}\psi_{m,k}^*(\mathbf{r})\frac{\partial}{\partial z}\psi_{m,k}(\mathbf{r}).$$

We now formulate an expansion for a k-dependent inclusion permittivity without coupling between modes. This is the situation in an electron gas, where the physical permittivity value is associated with each mode [21]. We first write the response of the inclusion to an excitation at a given k:

$$\psi_{\mathrm{sc},k} = \frac{u_{zk}\Gamma_z}{1-u_{zk}\Gamma_z}\psi_{0k},$$

where u_{zk} corresponds to the physical inclusion permittivity at a given k and

$$\psi_{0k} = \langle\psi_0|\psi_k\rangle\psi_k.$$

We can now sum these terms and substitute in the expansion above $s_z \to s_z(m,k)$ to obtain for a cylindrical inclusion

$$\psi = \psi_0 + \frac{4\pi}{\epsilon_2}\sum_m \int \frac{s_{z,km}^2}{s_z(m,k) - s_{z,km}} |\psi_{km}\rangle\nabla\psi_{km}^*(\mathbf{r}_0)\cdot\mathbf{p}dk. \tag{A2}$$

Note that the previous expansion for the electric potential with a uniform inclusion permittivity is satisfied for each k component, which implies that one can vary ϵ as a function of k in the expansion.

Finally, we analyze the response of a crystal inclusion. In the case of a helical crystal the Fourier expansion is along a helical orbit and the dc components have constant potential along this orbit. We thus have coupling between modes of the types [33] $(m',k') \to (m'+pm, k'+pmk_z)$ and $(m',k') \to (m', k'+pnk_z)$, where p is an integer number and n is the number of units per helical round. We will show next that for $\rho_0 - \rho_2 > a/n$ and $a/2$, the second and first types of coupling are negligible, respectively. We therefore conclude that for $\rho_0 - \rho_2 > a/2$ only the $m=1$ mode is important and write

$$\begin{aligned}\psi(\boldsymbol{r}, \rho_0 > a/2) \approx \psi_0(\boldsymbol{r}) + \frac{4\pi}{\epsilon_2}\int \frac{s_{z,km=1}^2}{s_z(m=1,k) - s_{z,km=1}} \\ \times |\psi_{km}\rangle\nabla\psi_{km}^*(\mathbf{r}_0)\cdot\mathbf{p}dk.\end{aligned} \tag{A3}$$

We can substitute the eigenpermittivities and the physical permittivity, to get $s_z(m=1,k)$ and $s_{k,m=1}$, respectively, and obtain an expansion for $\psi(\mathbf{r})$. The calculation of the eigenpermittivities can be performed using the boundary conditions and the physical permittivity can be measured in some cases or calculated by substituting $\omega(k)$ in ω_T in the expression for ϵ. $\omega(k)$ is calculated in the main text from the EOM and can also be calculated when anharmonic terms are incorporated.

Since a strong response is expected at $m=1, k=k_z$, a dipole that emits at a range of spatial frequencies will interact more dominantly with this mode. In this region the dominant term in the expansion is

$$\frac{4\pi}{\epsilon_2}\frac{s_{k_z m=1}^2}{s_z(m=1,k_z) - s_{k_z m=1}} |\psi_{k_z m=1}\rangle\nabla\psi_{k_z m=1}^*(\mathbf{r}_0)\cdot\mathbf{p},$$

in addition to ψ_0, where $k_z = \frac{2\pi}{a}$ and a is the helical-orbit axial periodicity.

2. The form of the eigenfunctions

Since a $\boldsymbol{E}_{\mathrm{inc}}/\psi_0$ component with a given k results in a contribution of an eigenfunction with the same k in the expansion, the eigenfunctions that account for the field scattering due to synchronous vibrations are

$$\psi_m = e^{im(\phi - k_z z)}\begin{cases} A_{1m}K_m(mk_z\rho) & \rho > \rho_2 \\ A_{2m}I_m + A_{3m}K_m & \rho_1 < \rho < \rho_2 \\ A_{4m}I_m(mk_z\rho) & \rho < \rho_1 \end{cases},$$

where ϕ, z, and ρ are cylindrical-coordinate variables, I_m and K_m are the modified Bessel functions, ρ_1 and ρ_2 are the internal and external inclusion radii, $k_z = 2\pi/a$, and a is the helical-orbit axial period. Upon a continuous translation along the helical orbit, ψ_m remains constant and therefore corresponds to an eigenvalue 1. We can similarly take the directional derivative in the direction of the helical orbit and obtain

$$\begin{aligned}\nabla_v\psi_m = v\cdot\nabla\psi_m = -\frac{i}{\sqrt{(\rho k_z)^2+1}} \\ \times (\rho k_z, 1)\cdot(m/\rho, -mk_z)e^{im(\phi-k_z z)} = 0,\end{aligned}$$

as expected. This means that $\hat{R}\psi_n = \psi_n$, where $\hat{R}$ is the continuous-translation operator.

3. Scaling of the eigenfunctions

We analyze the scaling of ψ_m for small and large ρs. We start with the first $m=0$ mode:

$$K_m(x\to 0) \to \begin{cases} -\left[\ln\left(\frac{x}{2}\right) + 0.5772\right] & m=0 \\ \frac{\Gamma(m)}{2}\left(\frac{2}{x}\right)^m & m\neq 0 \end{cases}.$$

Since, for $m = 0, x = 0$ and we expect a finite potential, this mode is associated in all regions with $I_{m=0}(x)$ and is constant everywhere (and therefore can be omitted). This mode can be treated in the full Maxwell-equation analysis and was shown to scale as $\sqrt{1/\rho}$ [41]. We proceed to the $m \geqslant 1$ modes at $\rho \gg a$ and obtain

$$K_{m\geqslant 1}(mk_z\rho \gg a) \to \frac{1}{\sqrt{2mk_z}}\sqrt{\frac{\pi}{\rho}}e^{-mk_z\rho},$$

with a typical interaction distance on the order of a/m. This determines the range in which a dipole interacts with each mode. When k and m are large this approximation holds and one can show that $\lim_{k,m\to\infty}\frac{|\nabla\psi_{m,k\mu}(\boldsymbol{r}_0)|^2}{\langle\psi_m|\psi_m\rangle} \propto mk\epsilon_{1k}e^{-2km\rho_0}$. Taking into account that $\mathrm{Im}[\epsilon_1(k)] > 0$, $\frac{s_m^2\mathrm{Im}(s^*)}{\{\mathrm{Re}[s(k')]-s_m(k')\}^2+[\mathrm{Im}(s)]^2}$ is bounded since even at the limit $s_m \to \infty$ it equals 1, and that ϵ_{1k} should converge when $k \to \infty$ (see the Appendix in Ref. [19]) the integral over k' and sum over m in Eq. (10) are ensured to converge. Clearly, the larger ρ_0 is, the faster it converges.

The scaling of the helical modes inside the structure close to the origin is

$$I_m(x \to 0) \to \frac{1}{\Gamma(m+1)}\left(\frac{x}{2}\right)^m,$$

$$I_{m=0}(mk_z\rho \to 0) \to \frac{1}{\Gamma(m+1)}\left(\frac{mk_z\rho}{2}\right)^m \propto m^m\left(\frac{k_z\rho}{2}\right)^m, \quad \Gamma(m+1) = m!.$$

4. Calculating the radial argument inside the inclusion

In a crystal one can express the effective permittivity as $\epsilon = \epsilon(\omega, k)$, which relates the response at a given k to an excitation at the same k. In the case of a MT, this form of $\epsilon(\omega, k)$ is justified because the period length a is 8 nm and, therefore, $(\lambda_0/a)^2 \gg 1$ where $\lambda_0 = c/\omega$ is the vacuum wavelength [20]. Note that in the derivation in Ref. [20] it is assumed that, inside the inclusion $\rho_{\mathrm{ext}}(\omega) = 0, \boldsymbol{J}_{\mathrm{ext}}(\omega) = 0$, which is satisfied in our case since the charges on the tubulin and tubulin dimers oscillate only as a response to an external excitation and can therefore be defined as polarization. Also, eigenstates are defined for a system without a source. Another argument is that for sources at distances larger than the typical interaction distance of the $m = 2$ mode the inclusion is approximately not affected by the $m > 1$ modes.

To represent axial vibrations, we assume an anisotropic inclusion with an axial permittivity ϵ_z and radial and azimuthal permittivities ϵ_2, equal to the host-medium permittivity, where we omit k for brevity. Note that the eigenpermittivities in the quasistatic regime do not depend on ω. We now solve Laplace's equation in cylindrical coordinates inside the anisotropic inclusion. This will allow us to find the argument of the functions I_m and K_m for $\rho_1 < \rho < \rho_2$ and calculate the eigenpermittivities. Substituting the form of ψ_m we write Laplace's equation inside the helical structure:

$$\nabla\overleftrightarrow{\epsilon}\nabla\psi_m = 0,$$
$$\epsilon_2\frac{1}{\rho}\frac{\partial}{\partial\rho}\left(\rho\frac{\partial\psi_m}{\partial\rho}\right) - \epsilon_2 m^2\frac{1}{\rho^2}\psi_m - k_z^2m^2\epsilon_{zm}\psi_m = 0. \quad \text{(A4)}$$

We change variables

$$x \equiv km\sqrt{\epsilon_z/\epsilon_2}\rho, \quad \frac{\partial}{\partial\rho} = \frac{\partial}{\partial x}\frac{\partial x}{\partial\rho} = \frac{\partial}{\partial x}k_zm\sqrt{\epsilon_{zm}/\epsilon_2},$$

and write

$$\frac{1}{x}k_z^2m^2\epsilon_{zm}\frac{\partial}{\partial x}\left(x\frac{\partial\psi_m}{\partial x}\right) - m^2\frac{(k_zm\sqrt{\epsilon_{zm}})^2}{x^2}\psi_m - k_z^2m^2\epsilon_{zm}\psi_m = 0,$$
$$\frac{1}{x}\frac{\partial}{\partial x}\left(x\frac{\partial\psi_m}{\partial x}\right) - \left(\frac{m^2}{x^2}\psi_m + 1\right)\psi_m = 0. \quad \text{(A5)}$$

Thus we get

$$\psi_m = e^{im(\phi-k_zz)}\begin{cases} A_{1m}K_m(mk_z\rho) & \rho > \rho_2 \\ A_{2m}I_m\left(mk_z\sqrt{\frac{\epsilon_{zm}}{\epsilon_2}}\rho\right) + A_{3m}K_m\left(mk_z\sqrt{\frac{\epsilon_{zm}}{\epsilon_2}}\rho\right) & \rho_1 < \rho < \rho_2, \\ A_{4m}I_m(mk_z\rho) & \rho < \rho_1 \end{cases}$$

which needs to be multiplied by additional factors to obtain the contribution in the expansion of the potential of a point charge as we showed in the previous subsection. Note that when calculating the total response as in Eqs. (2), (5), and (10) one has to sum over m and integrate over k for any relation between k and m.

5. Isotropic cylindrical shell: Calculating the eigenpermittivities

We express the eigenvalue equation and the relations between the coefficients of the eigenfunctions of an isotropic cylindrical shell:

$$\psi_{m,k} = e^{i(m\phi+kz)}\begin{cases} AK_m(k\rho) & \rho > \rho_2 \\ B_1I_m(k\rho) + B_2K_m(k\rho) & \rho_1 < \rho < \rho_2, \\ C_1I_m(k\rho) & \rho < \rho_1 \end{cases}$$

where B_1 is treated as known (and cancels out in the expansion). We first write the boundary

conditions

$$\begin{aligned} Aa &= B_1 b_{11} + B_2 b_{21}, \\ B_1 b_{12} + B_2 b_{22} &= C_1 c, \\ A\epsilon_2 a_d &= \epsilon_1 (B_1 b_{11d} + B_2 b_{21d}), \\ \epsilon_1 (B_1 b_{12d} + B_2 b_{22d}) &= C_1 \epsilon_2 c_d, \end{aligned}$$

where

$$\begin{aligned} &a = I_m(k\rho_1), \quad b_{11}^{\pm} = I_m(k\rho_1), \quad b_{12}^{\pm} = I_m(k\rho_2), \\ &b_{21}^{\pm} = K_m(k\rho_1), \quad b_{22}^{\pm} = K_m(k\rho_2), \quad c = K_m(k\rho_2), \\ &a_d = \epsilon_2 \left(\frac{\partial I_m(k\rho)}{\partial \rho} \right)_{\rho=\rho_1}, b_{11d}^{\pm} = \epsilon_1 \left(\frac{\partial}{\partial \rho} I_m(k\rho) \right)_{\rho=\rho_1}, \\ &b_{12d}^{\pm} = \left(\frac{\partial}{\partial \rho} I_m(k\rho) \right)_{\rho=\rho_2}, b_{21d}^{\pm} = \epsilon_1 \left(\frac{\partial}{\partial \rho} K_m(k\rho) \right)_{\rho=\rho_1}, \\ &b_{22d}^{\pm} = \epsilon_1 \left(\frac{\partial}{\partial \rho} K_m(k\rho) \right)_{\rho=\rho_2}, \quad c_d = \epsilon_2 \left(\frac{\partial K_m(k\rho)}{\partial \rho} \right)_{\rho=\rho_2}. \end{aligned}$$

We write two relations between B_2 and ϵ_1

$$\epsilon_1 (B_1 b_{12d} + B_2 b_{22d}) = \epsilon_2 \frac{B_1 b_{12} + B_2 b_{22}}{c} c_d, \tag{A6}$$

$$\frac{B_1 b_{11} + B_2 b_{21}}{a} a_d \epsilon_2 = \epsilon_1 (B_1 b_{11d} + B_2 B_{21d}), \tag{A7}$$

and express B_2

$$\begin{aligned} \epsilon_1 B_2 b_{22d} - \epsilon_2 \frac{B_2 b_{22} c_d}{c} &= \epsilon_2 \frac{B_1 b_{12}}{c} c_d - \epsilon_1 B_1 b_{12d}, \\ B_2 \left(\epsilon_1 b_{22d} - \epsilon_2 \frac{b_{22} c_d}{c} \right) &= B_1 (\epsilon_2 \frac{b_{12}}{c} c_d - \epsilon_1 b_{12d}), \\ B_2 &= B_1 \left(\frac{\epsilon_2 \frac{b_{12}}{c} c_d - \epsilon_1 b_{12d}}{\epsilon_1 b_{22d} - \epsilon_2 \frac{b_{22} c_d}{c}} \right). \end{aligned}$$

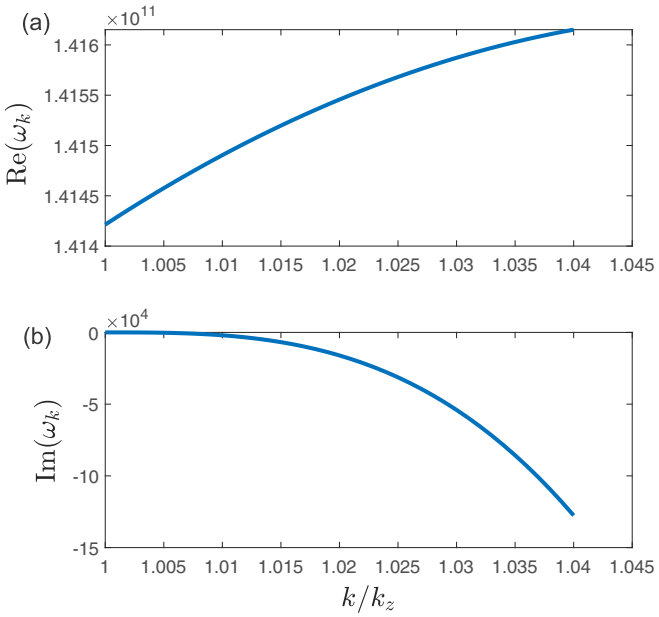

FIG. 6. (a) Real part of ω_k and (b) imaginary part of ω_k, where the coefficient of the anharmonic term is $k_5 = 5k_3k_z$ and the mode amplitude is $u_1 = 0.1a$.

Substituting B_2 we obtain a quadratic eigenvalue equation for ϵ_1:

$$\begin{aligned} 0 = &\frac{\epsilon_1}{\epsilon_2} b_{22d} \left(b_{11d} \frac{\epsilon_1}{\epsilon_2} - b_{11} \frac{a_d}{a} \right) - \frac{b_{22} c_d}{c} \left(b_{11d} \frac{\epsilon_1}{\epsilon_2} - b_{11} \frac{a_d}{a} \right) \\ &+ \frac{b_{12}}{c} c_d \left(\frac{\epsilon_1}{\epsilon_2} b_{21d} - b_{21} \frac{a_d}{a} \right) - \frac{\epsilon_1}{\epsilon_2} b_{12d} \left(\frac{\epsilon_1}{\epsilon_2} b_{21d} - b_{21} \frac{a_d}{a} \right). \end{aligned}$$

Finally, we express A and C_1

$$\begin{aligned} A &= B_1 \frac{b_{11} + \left(\frac{\epsilon_2 \frac{b_{12}}{c} c_d - \epsilon_1 b_{12d}}{\epsilon_1 b_{22d} - \epsilon_2 \frac{b_{22} c_d}{c}} \right) b_{21}}{a}, \\ C_1 &= B_1 \frac{b_{12} + \left(\frac{\epsilon_2 \frac{b_{12}}{c} c_d - \epsilon_1 b_{12d}}{\epsilon_1 b_{22d} - \epsilon_2 \frac{b_{22} c_d}{c}} \right) b_{22}}{c}, \end{aligned}$$

and obtain the two sets of solutions:

$$\begin{aligned} A = &-\frac{B_1}{2a(ab_{22}b_{21d}c_d - b_{21}ca_d b_{22d})} \{ -cb_{21}^2 a_d b_{12d} + b_{11}b_{21}ca_d b_{22d} + ab_{22}b_{21}b_{11d}c_d + ab_{12}b_{21}b_{21d}c_d + -2ab_{11}b_{22}b_{21d}c_d \\ &\pm b_{21} \sqrt{[ca_d(b_{21}b_{12d} - b_{11}b_{22d}) + a(b_{12}b_{21d} - b_{22}b_{11d})c_d]^2 - 4a(b_{12}b_{21} - b_{11}b_{22})ca_d(b_{12d}b_{21d} - b_{11d}b_{22d})c_d} \}, \\ B_2 = &\frac{B_1}{2b_{21}ca_d b_{22d} - 2ab_{22}b_{21d}c_d} \{ -b_{21}ca_d b_{12d} - b_{11}ca_d b_{22d} + ab_{22}b_{11d}c_d + ab_{12}b_{21d}c_d \\ &\pm \sqrt{[ca_d(b_{21}b_{12d} - b_{11}b_{22d}) + a(b_{12}b_{21d} - b_{22}b_{11d})c_d]^2 - 4a(b_{12}b_{21} - b_{11}b_{22})ca_d(b_{12d}b_{21d} - b_{11d}b_{22d})c_d} \}, \\ C = &\frac{B_1}{2c(b_{21}ca_d b_{22d} - ab_{22}b_{21d}c_d)} \{ ab_{22}^2 b_{11d}c_d - b_{21}b_{22}ca_d b_{12d} - b_{11}b_{22}ca_d b_{22d} - ab_{12}b_{22}b_{21d}c_d + 2b_{12}b_{21}ca_d b_{22d} \\ &\pm b_{22} \sqrt{[ca_d(b_{21}b_{12d} - b_{11}b_{22d}) + a(b_{12}b_{21d} - b_{22}b_{11d})c_d]^2 - 4a(b_{12}b_{21} - b_{11}b_{22})ca_d(b_{12d}b_{21d} - b_{11d}b_{22d})c_d} \}, \\ \epsilon_{1k}/\epsilon_2 = &-\frac{1}{2ac(b_{12d}b_{21d} - b_{11d}b_{22d})} \{ -b_{21}ca_d b_{12d} + b_{11}ca_d b_{22d} + ab_{22}b_{11d}c_d - ab_{12}b_{21d}c_d + \\ &\pm \sqrt{[ca_d(b_{21}b_{12d} - b_{11}b_{22d}) + a(b_{12}b_{21d} - b_{22}b_{11d})c_d]^2 - 4a(b_{12}b_{21} - b_{11}b_{22})ca_d(b_{12d}b_{21d} - b_{11d}b_{22d})c_d} \}. \end{aligned}$$

6. Including anharmonicity

Here we calculated ω_k when anharmonicity in the axial forces between lateral units is included in the model without dispersion, where we set the amplitude $u_1 = 0.1a$ for simplicity, see Fig. 6. It can be seen that $\mathrm{Im}(\omega_k)$ increases away from $k = k_z$, which implies a stronger and delocalized response when $k \approx k_z$, since the physical frequency is real. A complete account of this analysis as a function of the incoming field will be given elsewhere.

[1] M. S. Dresselhaus, A. Jorio, M. Hofmann, G. Dresselhaus, and R. Saito, Perspectives on carbon nanotubes and graphene raman spectroscopy, Nano Lett. **10**, 751 (2010).

[2] A. Mershin, A. A. Kolomenski, H. A. Schuessler, and D. V. Nanopoulos, Tubulin dipole moment, dielectric constant and quantum behavior: Computer simulations, experimental results and suggestions, Biosystems **77**, 73 (2004).

[3] J. Preto, M. Pettini, and J. A. Tuszynski, Possible role of electrodynamic interactions in long-distance biomolecular recognition, Phys. Rev. E **91**, 052710 (2015).

[4] J. Tuszynski, T. Luchko, E. Carpenter, and E. Crawford, Results of molecular dynamics computations of the structural and electrostatic properties of tubulin and their consequences for microtubules, J. Comput. Theor. Nanosci. **1**, 392 (2004).

[5] J. R. Guzman-Sepulveda, R. Wu, A. P. Kalra, M. Aminpour, J. A. Tuszynski, and A. Dogariu, Tubulin polarizability in aqueous suspensions, ACS Omega **4**, 9144 (2019).

[6] J. A. Tuszynski, C. Wenger, D. E. Friesen, and J. Preto, An overview of sub-cellular mechanisms involved in the action of ttfields, Int. J. Environ. Res. Public Health **13**, 1128 (2016).

[7] M. Cifra, J. Pokorný, D. Havelka, and O. Kučera, Electric field generated by axial longitudinal vibration modes of microtubule, Biosystems **100**, 122 (2010).

[8] K. A. Thackston, D. D. Deheyn, and D. F. Sievenpiper, Simulation of electric fields generated from microtubule vibrations, Phys. Rev. E **100**, 022410 (2019).

[9] D. J. Bergman and D. Stroud, Theory of resonances in the electromagnetic scattering by macroscopic bodies, Phys. Rev. B **22**, 3527 (1980).

[10] C. Sauvan, J.-P. Hugonin, I. Maksymov, and P. Lalanne, Theory of the Spontaneous Optical Emission of Nanosize Photonic and Plasmon Resonators, Phys. Rev. Lett. **110**, 237401 (2013).

[11] A. Farhi and D. J. Bergman, Electromagnetic eigenstates and the field of an oscillating point electric dipole in a flat-slab composite structure, Phys. Rev. A **93**, 063844 (2016).

[12] D. J. Bergman, The dielectric constant of a simple cubic array of identical spheres, J. Phys. C **12**, 4947 (1979).

[13] D. J. Bergman, in *Les Methodes de lHomogeneisation: Theorie et Applications en Physiques*, edited by R. Dautray (Editions Eyrolles, Paris, 1985).

[14] N. Fang, H. Lee, C. Sun, and X. Zhang, Sub–diffraction-limited optical imaging with a silver superlens, Science **308**, 534 (2005).

[15] A. Farhi and D. J. Bergman, Eigenstate expansion of the quasistatic electric field of a point charge in a spherical inclusion structure, Phys. Rev. A **96**, 043806 (2017).

[16] M. Jablan, H. Buljan, and M. Soljačić, Plasmonics in graphene at infrared frequencies, Phys. Rev. B **80**, 245435 (2009).

[17] R. Hillenbrand, T. Taubner, and F. Keilmann, Phonon-enhanced light–matter interaction at the nanometre scale, Nature (London) **418**, 159 (2002).

[18] V. Klimov and M. Ducloy, Spontaneous emission rate of an excited atom placed near a nanofiber, Phys. Rev. A **69**, 013812 (2004).

[19] A. Farhi and A. Dogariu, Coupling of electrodynamic fields to vibrational modes in helical structures, Phys. Rev. A **103**, 023523 (2021).

[20] V. M. Agranovich and V. Ginzburg, *Crystal Optics with Spatial Dispersion, and Excitons* (Springer, New York, 2013), Vol. 42.

[21] C. Kittel, P. McEuen, and P. McEuen, *Introduction to Solid State Physics* (Wiley, New York, 1996), Vol. 8.

[22] R. Carminati, A. Cazé, D. Cao, F. Peragut, V. Krachmalnicoff, R. Pierrat, and Y. De Wilde, Electromagnetic density of states in complex plasmonic systems, Surf. Sci. Rep. **70**, 1 (2015).

[23] K. Joulain, R. Carminati, J.-P. Mulet, and J.-J. Greffet, Definition and measurement of the local density of electromagnetic states close to an interface, Phys. Rev. B **68**, 245405 (2003).

[24] M. González-Jiménez, G. Ramakrishnan, T. Harwood, A. J. Lapthorn, S. M. Kelly, E. M. Ellis, and K. Wynne, Observation of coherent delocalized phonon-like modes in dna under physiological conditions, Nat. Commun. **7**, 11799 (2016).

[25] A. Cazé, R. Pierrat, and R. Carminati, Spatial Coherence in Complex Photonic and Plasmonic Systems, Phys. Rev. Lett. **110**, 063903 (2013).

[26] R. Carminati, J.-J. Greffet, C. Henkel, and J.-M. Vigoureux, Radiative and non-radiative decay of a single molecule close to a metallic nanoparticle, Opt. Commun. **261**, 368 (2006).

[27] N. Rivera, I. Kaminer, B. Zhen, J. D. Joannopoulos, and M. Soljačić, Shrinking light to allow forbidden transitions on the atomic scale, Science **353**, 263 (2016).

[28] E. Purcell, Spontaneous emission probabilities at radio frequencies, Phys. Rev. **69**, 681 (1946).

[29] H. T. Dung, L. Knöll, and D.-G. Welsch, Intermolecular energy transfer in the presence of dispersing and absorbing media, Phys. Rev. A **65**, 043813 (2002).

[30] F. Wijnands, J. B. Pendry, F. J. Garcia-Vidal, P. M. Bell, P. J. Roberts, and L. M. Moreno, Green's functions for Maxwell's equations: Application to spontaneous emission, Opt. Quantum Electron. **29**, 199 (1997).

[31] E. N. Economou, *Green's Functions in Quantum Physics* (Springer, New York, 1983), Vol. 3.

[32] A. Yariv and P. Yeh, *Optical Waves in Crystals* (Wiley, New York, 1984), Vol. 5.

[33] G. Edwards, D. Hochberg, and T. W. Kephart, Structure in the electric potential emanating from dna, Phys. Rev. E **50**, R698 (1994).

[34] J. Kimball, C. Fong, and Y. Shen, Anharmonicity, phonon localization, two-phonon bound states, and vibrational spectra, Phys. Rev. B **23**, 4946 (1981).

[35] C. Hess, M. Wolf, and M. Bonn, Direct Observation of Vibrational Energy Delocalization on Surfaces: CO on Ru(001), Phys. Rev. Lett. **85**, 4341 (2000).

[36] S. Portet, J. Tuszyński, C. Hogue, and J. Dixon, Elastic vibrations in seamless microtubules, Eur. Biophys. J. **34**, 912 (2005).

[37] M. Van den Heuvel, M. De Graaff, S. Lemay, and C. Dekker, Electrophoresis of individual microtubules in microchannels, Proc. Natl. Acad. Sci. USA **104**, 7770 (2007).

[38] P. J. de Pablo, I. A. Schaap, F. C. MacKintosh, and C. F. Schmidt, Deformation and Collapse of Microtubules on the Nanometer Scale, Phys. Rev. Lett. **91**, 098101 (2003).

[39] S. Sahu, S. Ghosh, B. Ghosh, K. Aswani, K. Hirata, D. Fujita, and A. Bandyopadhyay, Atomic water channel controlling remarkable properties of a single brain microtubule: Correlating single protein to its supramolecular assembly, Biosens. Bioelectron. **47**, 141 (2013).

[40] D. J. Bergman, Perfect imaging of a point charge in the quasistatic regime, Phys. Rev. A **89**, 015801 (2014).

[41] D. Bergman, Electromagnetic eigenstates of finite cylinders and cylinder-clusters: Application to macroscopic response of metamaterials, Proc. SPIE **7032**, 70321A (2008).